Article

A Jovian analogue orbiting a white dwarf star

https://doi.org/10.1038/s41586-021-03869-6

Received: 17 September 2020

Accepted: 30 July 2021

Published online: 13 October 2021

Check for updates

J. W. Blackman[1,2]✉, J. P. Beaulieu[1,2], D. P. Bennett[3,4], C. Danielski[2,5,6], C. Alard[2], A. A. Cole[1], A. Vandorou[1], C. Ranc[3], S. K. Terry[7], A. Bhattacharya[3,4], I. Bond[8], E. Bachelet[9], D. Veras[10,11,12], N. Koshimoto[3,13], V. Batista[2] & J. B. Marquette[14]

Studies[1,2] have shown that the remnants of destroyed planets and debris-disk planetesimals can survive the volatile evolution of their host stars into white dwarfs[3,4], but few intact planetary bodies around white dwarfs have been detected[5–8]. Simulations predict[9–11] that planets in Jupiter-like orbits around stars of $\lesssim 8\,M_{\odot}$ (solar mass) avoid being destroyed by the strong tidal forces of their stellar host, but as yet, there has been no observational confirmation of such a survivor. Here we report the non-detection of a main-sequence lens star in the microlensing event MOA-2010-BLG-477Lb[12] using near-infrared observations from the Keck Observatory. We determine that this system contains a $0.53 \pm 0.11\,M_{\odot}$ white-dwarf host orbited by a 1.4 ± 0.3 Jupiter-mass planet with a separation on the plane of the sky of 2.8 ± 0.5 astronomical units, which implies a semi-major axis larger than this. This system is evidence that planets around white dwarfs can survive the giant and asymptotic giant phases of their host's evolution, and supports the prediction that more than half of white dwarfs have Jovian planetary companions[13]. Located at approximately 2.0 kiloparsecs towards the centre of our Galaxy, it is likely to represent an analogue to the end stages of the Sun and Jupiter in our own Solar System.

The microlensing event MOA-2010-BLG-477Lb was first detected by the Microlensing Observations in Astrophysics collaboration on 2 August 2010 (ref. [12]). Microlensing is a technique that is sensitive to cold planets down to the mass of Earth[14] and can probe objects around all kinds of stars, including white dwarfs; unlike other detection methods, it does not rely on the light coming from the host. MOA-2010-BLG-477 is a planetary microlensing event with a planet–host mass ratio of $q = (2.61 \pm 0.03) \times 10^{-3}$ and a large Einstein ring radius $\theta_E = 1.26 \pm 0.06$ milliarseconds (mas), which implies a host star that is relatively massive or nearby.

The target was subsequently observed with the near-infrared camera 2 (NIRC2) instrument on the Keck-II telescope on 27 July 2015, 5 August 2016, and 23 May 2018 in the H and K_s near-infrared bands (1.5–2.3 μm) using laser guide star adaptive optics. Data were obtained with the wide camera (40 arcsec field of view (FOV)) for calibration, and the narrow camera (10 arcsec FOV) in an attempt to resolve the source and lens. Assuming it sits on the main sequence, we predict a host star with a mass of $0.15\,M_{\odot} < M_L < 0.93\,M_{\odot}$ (solar mass $M_{\odot} = 1.99 \times 10^{30}$ kg) orbited by a planet with mass $0.5\,M_J < m_p < 2.1\,M_J$ (Jupiter mass, $M_J = 1.898 \times 10^{27}$ kg) at a distance of $0.7 < D_L < 2.7$ kpc (1 kpc = 3×10^{16} km) if all stellar types are equally likely to host a planet. Modelled parameters of the microlensing light curve and the source magnitude and colour[15] yield a lens–source relative proper motion of $\mu_{rel,G} = 11.53 \pm 0.56$ mas yr^{-1}. This prediction, presented here in the geocentric reference frame that moves with the Earth's velocity at the time of the event, allows us to estimate the future lens–source separation following the event's peak on 12 August 2010.

In our Keck images, we find an $H = 18.52 \pm 0.05$ star located 123 mas to the northeast (hereafter star 123NE, Fig. 1c, top left)) of the source. Given the large lens–source relative proper motion, a predicted separation of 57 mas means the lens star should have been detectable under ideal observing conditions in 2015, 4.96 years after the event peak. By 2018, this separation should have widened to 90 mas. We find that the separation of star 123NE has actually decreased by 11.5 mas between 2015 and 2018, instead of the expected 33 mas increase if it were the lens. The direction of this proper motion indicates that this object is unrelated to the lens and the planetary system.

The source magnitude was measured as $H_s = 17.32 \pm 0.03$ and $K_s = 17.17 \pm 0.04$ using data from the Cerro Tololo Inter-American Observatory (CTIO) and the Vista Variables in the Via Lactea (VVV) survey. This brightness is compatible with our Keck/NIRC2 images, determined using the flux ratio between star 123NE and the star at the position of the source. The sum of the two stars (shown in Fig. 1c) is $K = 16.78 \pm 0.02$ using the Keck data and $K = 16.79 \pm 0.03$ using the CTIO data. This is consistent with the absence of excess flux within the point spread function (PSF) of the source star. To confirm this, we modelled the PSF with the addition of weak contributions from the wings of the unrelated companion, and found no significant structure in the residuals. Hence, with no evidence of a detectable lens in our Keck/NIRC2 images, the lens star must have a brightness below the detection limit.

To determine this limit, we define the detection to be above the noise at the 3σ level. This corresponds to a threshold of $H \approx 21.1$, which means

[1]School of Natural Sciences, University of Tasmania, Hobart, Australia. [2]Sorbonne Universités, UPMC Université Paris 6 et CNRS, UMR 7095, Institut d'Astrophysique de Paris, Paris, France. [3]Laboratory for Exoplanets and Stellar Astrophysics, NASA/Goddard Space Flight Center, Greenbelt, MD, USA. [4]Department of Astronomy, University of Maryland, College Park, MD, USA. [5]Instituto de Astrofísica de Andalucía (IAA-CSIC), Granada, Spain. [6]UCL Centre for Space Exochemistry Data, Didcot, UK. [7]Department of Astronomy, University of California Berkeley, Berkeley, CA, USA. [8]Institute for Natural and Mathematical Sciences, Massey University, Auckland, New Zealand. [9]Las Cumbres Observatory, Goleta, CA, USA. [10]Centre for Exoplanets and Habitability, University of Warwick, Coventry, UK. [11]Department of Physics, University of Warwick, Coventry, UK. [12]Centre for Space Domain Awareness, University of Warwick, Coventry, UK. [13]Department of Astronomy, Graduate School of Science, The University of Tokyo, Tokyo, Japan. [14]Laboratoire d'Astrophysique de Bordeaux, University of Bordeaux, Pessac, France. ✉e-mail: joshua.blackman@utas.edu.au

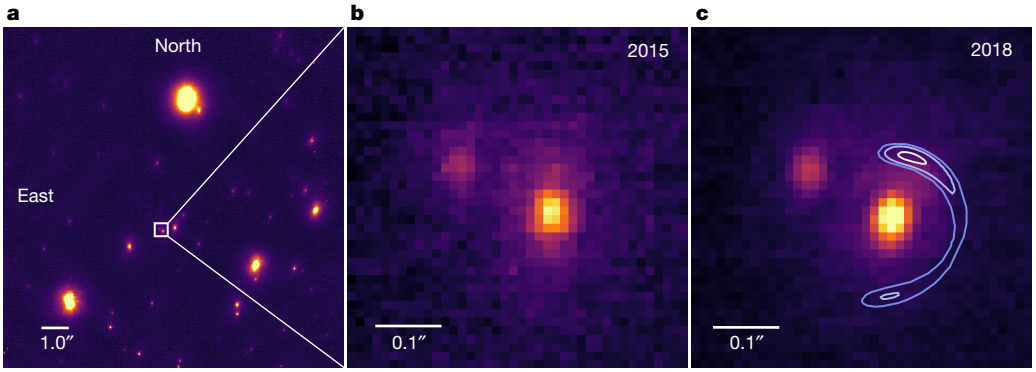

Fig. 1 | *H*-band adaptive optics imaging of MOA-2010-BLG-477 from the Keck Observatory. a, An image obtained with the narrow-camera on the NIRC2 imager in 2015 centred on MOA-2010-BLG-477 with an FOV of 8 arcsec. **b**, A 0.36-arcsec zoomed-in view of the same image as in **a**. The bright object in the centre is the source. To the northeast (top left) is an unrelated $H = 18.52 \pm 0.05$ star 123 mas from the source, which we refer to as star 123NE. **c**, The field in 2018. The contours indicate the probable positions of a possible main-sequence host (probability of 0.393, 0.865, 0.989 from light to dark blue) using constraints from microlensing parallax and lens–source relative proper motion. No such host is detected.

that any object brighter than this value should be detectable within our Keck narrow frames. This limit includes an extinction correction of $A_H = 0.21$. The light curve of this event indicates a microlensing parallax signal due to the orbital motion of the Earth, but it is not fully constrained. This implies that for each light curve model in our Markov chain distribution, we can determine the lens mass $M_L = (c^2/4G)(\theta_E/\pi_E)$[16], where π_E is the microlensing parallax, c is the speed of light and G is the gravitational constant. We combine these light-curve constraints with limits on the source and lens distances and velocities, together with an empirical mass–luminosity relation[17], and find that a main-sequence lens star must have a brightness of $H < 18.10$ at 99.0% confidence. This is largely due to the light-curve constraint on the angular Einstein ring radius, θ_E, derived from the angular radius of the source star and Einstein ring crossing time.

The measurement of the microlensing parallax and relative proper motion of the lens and source stars constrain the location of a main-sequence lens star to the interior of the contours shown in Fig. 1c. The predicted brightness of a main-sequence lens as a function of the lens distance is shown in Fig. 2. As all of the possible main-sequence lenses for the event are brighter than the Keck detection limit and no such star is observed, the lens cannot be a main-sequence star. The same analysis also excludes brown dwarf lenses owing to an upper limit on the microlensing parallax parameter, $\pi_E < 1.03$, which leads to an implied limit on the lens system mass of $M_L > 0.15\,M_\odot$. Similarly, the lower microlensing parallax limit of $\pi_E > 0.26$ implies an upper mass limit of $M_L < 0.78\,M_\odot$, which rules out neutron stars and black holes as the host stars. As main-sequence stars, brown dwarfs, neutron stars and black holes are ruled out, we conclude that the lens must be a white dwarf.

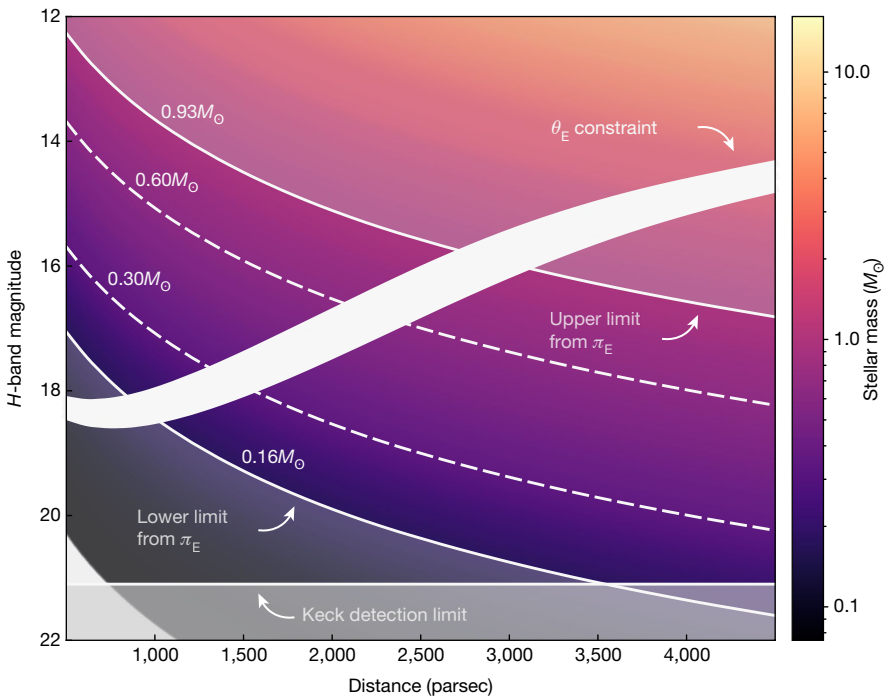

Fig. 2 | *H*-band brightness of possible main-sequence host lenses. In white is the Einstein ring radius constraint, θ_E, derived from finite source effects in the event light curve. This constraint indicates that if the planet host star was on the main sequence, it should be visible with Keck adaptive optics as the entire area lies above the detection threshold of our H-band images at $H \approx 21.1$. The mass–luminosity relations for different main-sequence lens masses are shown: $1.00M_\odot$, $0.50M_\odot$, $0.30M_\odot$, with $0.16M_\odot$ as the lower limit of the mass derived from the mircrolens parallax, π_E. Our null detection in our Keck images implies that the exoplanet host must be a stellar remnant, most probably a white dwarf.

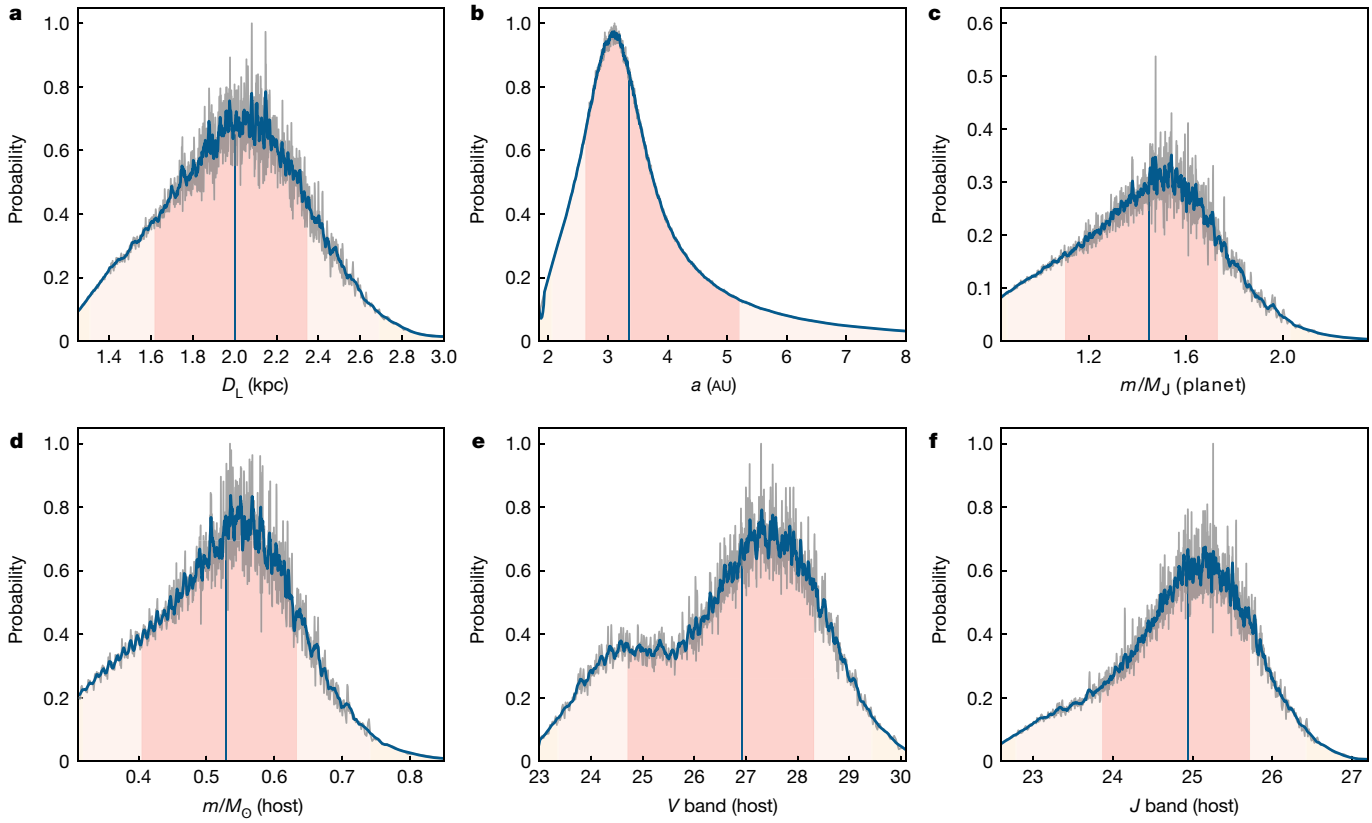

Fig. 3 | Physical properties of MOA-2010-BLG-477. a–f, Predicted distance to the host star–lens planetary system (**a**), three-dimensional star–planet separation (**b**), mass of the planet (**c**), mass of the host (**d**), predicted host star brightness in V (**e**) and predicted host star brightness in J (**f**). These parameters were calculated using a Bayesian analysis with priors from the relative proper motion of disk and bulge lenses, lens-star mass function, and velocity distributions derived from a galactic model described in ref. [17]. The central red areas indicate the standard deviation (1σ).

To estimate the properties of a white dwarf host, we use the Galactic model from ref. [17] and a complete sample of 130 white dwarfs within 20 parsec (ref. [18]), excluding unresolved double white dwarfs and double white dwarf candidates identified in ref. [19]. This calculation was made under the assumption that all white dwarfs are equally likely to host planets. Our results are summarized in Fig. 3 and Table 1. We find a probable white-dwarf host mass $M = 0.53 \pm 0.11\,M_\odot$, which sits slightly below the peak of the single-white-dwarf mass distribution at 0.57–0.58 $M_\odot$ and excludes the high-mass tail[20]. This implies a Jovian planet of mass $m_p = 1.43 \pm 0.30\,M_J$ at a distance of $D_L = 1.99 \pm 0.35$ kpc.

With a separation from the white dwarf of $a = 3.4^{+1.8}_{-0.8}$ AU (assuming a random orientation), it is likely that the planet MOA-2010-BLG-477Lb formed at the same time as the host star and managed to survive the post-main-sequence evolution. The mass loss experienced by a star on the giant and asymptotic giant branches pushes the planet towards a wider orbit, but tidal forces can have the opposite effect when the star expands to radii ≥1 AU (ref. [21]). In rare cases, the tidal effect can nearly cancel the mass-loss effect, leaving a giant planet orbiting at a separation as small as about 2 AU, but this requires a fine-tuning of the parameters to prevent the planet from being engulfed by the star. Most white dwarfs in the Galactic disk are thought to have formed from stars with initial masses of 1–2.5 $M_\odot$ (ref. [21]), and the measured separation means that to avoid tidal engulfment, the mass of the progenitor star is probably <2 $M_\odot$. Jovian planets orbiting these stars are generally thought to move to orbital separations of >5 or 6 AU around the remnant white dwarfs[11,22]. Although this is larger than the projected separation of about 2.8 AU of MOA-2010-BLG-477Lb, in the region where microlensing has the highest sensitivity, the reduced detection probability for white dwarf planets might be compensated by a higher intrinsic planet occurrence for gas giant planets around massive stars[23].

Table 1 | System parameters of MOA-2010-BLG-477Lb

Parameter	Units	Value (±1σ)	2σ range
White dwarf lens distance	D_L (kpc)	1.99 ± 0.35	1.31–2.69
White dwarf lens mass	M_L ($M_\odot$)	0.53 ± 0.11	0.32–0.74
Planet mass	m_p (M_J)	1.43 ± 0.30	0.87–2.03
Source star distance	D_S (kpc)	7.8 ± 1.3	5.5–10.2
Two-dimensional star–planet separation	$a_\perp$ (AU)	2.8 ± 0.5	1.9–3.7
Three-dimensional star–planet separation	a (AU)	$3.4^{+1.8}_{-0.8}$	2.1–12.1
Mass ratio	q (10^{-3})	2.61 ± 0.03	2.55–2.67
White dwarf host, V_L	mag	26.92 ± 1.80	23.38–29.44
White dwarf host, J_L	mag	24.93 ± 0.91	22.80–26.41

Online content

Any methods, additional references, Nature Research reporting summaries, source data, extended data, supplementary information, acknowledgements, peer review information; details of author contributions and competing interests; and statements of data and code availability are available at https://doi.org/10.1038/s41586-021-03869-6.

1. Vanderburg, A. et al. A disintegrating minor planet transiting a white dwarf. *Nature* **526**, 546–549 (2015).
2. Manser, C. J. et al. A planetesimal orbiting within the debris disc around a white dwarf star. *Science* **364**, 66–69 (2019).

3. Villaver, E. & Livio, M. Can planets survive stellar evolution? *Astrophys. J.* **661**, 1192–1201 (2007).
4. Duncan, M. J. & Lissauer, J. J. The effects of post-main-sequence solar mass loss on the stability of our planetary system. *Icarus* **134**, 303–310 (1998).
5. Sigurdsson, S. et al. A young white dwarf companion to pulsar B1620-26: evidence for early planet formation. *Science* **301**, 193–196 (2003).
6. Vanderburg, A. et al. A giant planet candidate transiting a white dwarf. *Nature* **585**, 363–367 (2020).
7. Luhman, K. L., Burgasser, A. J. & Bochanski, J. J. Discovery of a candidate for the coolest known brown dwarf. *Astrophys. J. Lett.* **730**, L9 (2011).
8. Gaensicke, B. T. et al. Accretion of a giant planet onto a white dwarf. *Nature* **576**, 61–64 (2019).
9. Madappatt, N., De Marco, O. & Villaver, E. The effect of tides on the population of PN from interacting binaries. *Mon. Not. R. Astron. Soc.* **463**, 1040–1056 (2016).
10. Mustill, A. J. et al. Unstable low-mass planetary systems as drivers of white dwarf pollution. *Mon. Not. R. Astron. Soc.* **476**, 3939–3955 (2018).
11. Nordhaus, J. & Spiegel, D. S. On the orbits of low-mass companions to white dwarfs and the fates of the known exoplanets. *Mon. Not. R. Astron. Soc.* **432**, 500–505 (2013).
12. Bachelet, E. et al. MOA 2010-blg-477lb: constraining the mass of a microlensing planet from microlensing parallax, orbital motion, and detection of blended light. *Astrophys. J.* **754**, 73 (2012).
13. Schreiber, M. R. et al. Cold giant planets evaporated by hot white dwarfs. *Astrophys. J. Lett.* **887**, L4 (2019).
14. Bennett, D. P. & Rhie, S. H. Detecting Earth-mass planets with gravitational microlensing. *Astrophys. J.* **472**, 660–664 (1996).
15. Boyajian, T. S. et al. Stellar diameters and temperatures. III. Main sequence A, F, G, and K stars: additional high-precision measurements and empirical relations. *Astrophys. J.* **771**, 40 (2014); erratum **787**, 92 (2014).
16. Gaudi, B. S. Microlensing surveys for exoplanets. *Annu. Rev. Astron. Astr.* **50**, 411–453 (2012).
17. Bennett, D. P. et al. MOA-2011-BLG-262Lb: a sub-Earth-mass moon orbiting a gas giant primary or a high velocity planetary system in the galactic bulge. *Astrophys. J.* **785**, 155 (2014).
18. Giammichele, N., Bergeron, P. & Dufour, P. Know your neighborhood: a detailed model atmosphere analysis of nearby white dwarfs. *Astrophys. J. Suppl. S.* **199**, 29 (2012).
19. Toonen, S., Hollands, M., Gänsicke, B. T. & Boekholt, T. The binarity of the local white dwarf population. *Astron. Astrophys.* **602**, 16 (2017).
20. Tremblay, P. E. et al. The field white dwarf mass distribution. *Mon. Not. R. Astron. Soc.* **461**, 2100–2114 (2016).
21. Veras, D. Post-main-sequence planetary system evolution. *R. Soc. Open Sci.* **3**, 150571 (2016).
22. Mustill, A. J. & Villaver, E. Foretellings of Ragnarök: world-engulfing asymptotic giants and the inheritance of white dwarfs. *Astrophys. J.* **761**, 121 (2012).
23. Ghezzi, L., Montet, B. T. & Johnson, J. A. Retired A stars revisited: an updated giant planet occurrence rate as a function of stellar metallicity and mass. *Astrophys. J.* **860**, 109 (2018).

Methods

Observations

The microlensing event MOA-2010-BLG-477 was originally detected using the 1.8-m telescope at Mount John Observatory, New Zealand, on 2 August 2010, and subsequently observed by more than 20 telescopes[12]. To find the predicted magnitude of the source star, we refer to the *H*-band light curve obtained by the μFUN 1.3-m SMARTS telescope at the CTIO. We calibrate the light curve according to data from the VVV survey[24]. Using a single amplified CTIO *H*-band frame with an epoch corresponding to the available VVV data, we cross-identify between the two. We derive a source magnitude of $H_{\rm CTIO,source} = 17.32 \pm 0.03$. Given the intrinsic source colour of $(H-K)_0 = 0.07$, and using extinction corrections derived using the OGLE extinction calculator[25,26], $A_H = 0.21$ and $A_K = 0.13$, we find $K_{\rm CTIO,source} = 17.17 \pm 0.04$.

Located at (α, δ) = (18 h 06 m 07.47 s, −31°27′16.17″, J2000.0), we observed the event using the NIRC2 instrument on the Keck-II telescope located on Mauna Kea (Hawaii) with laser guide star adaptive optics. Seven dithered *H*-band images were obtained with the narrow camera on 27 July 2015 (Heliocentric Julian Date, HJD = 2457230.7), 4.96 years following the event peak. These images have a median full-width at half-maximum of 50 mas. During this same epoch, we obtained fourteen 95 mas K_s-band images with the wide camera and ten 50 mas *H*-band images with the narrow camera. The event was observed twice: (1) in 2016 (HJD = 2457605.0), with seventeen 50 mas *H*-band narrow images and two 90 mas *H*-band wide images; (2) in 2018, with sixteen 50 mas K_s-band narrow frames. The final 2018 observations were taken on 23 May 2018 (HJD = 2458262.4), 7.78 years after the maximum magnification.

The goal of these observations was to determine the composition of the source-lens blend by obtaining a refined photometric and astrometric solution. We apply flat-field and dark corrections using standard techniques[27,28]. The images were stacked using SWarp[29]. We identify the source + lens star as the bright object in Fig. 1c. Comparing this with the OGLE-III reference image of the BLG 176.8 field (Extended Data Fig. 1), it is evident that the OGLE star is a blend of four dimmer stars, the second brightest of which is the source + lens star. The OGLE star (number 119416) has an *I*-band magnitude of $I = 17.446 \pm 0.052$, which is consistent with the value of $I = 17.443 \pm 0.031$ from DoPHOT CTIO photometry[12].

We perform aperture photometry using SExtractor[30] on the wide *K*-band frame from 2015, using the narrow images to cross-calibrate the narrow frames, and find a *K*-band magnitude of the blend at the position of the source as $K_{\rm Blend} = 16.78 \pm 0.03$. The magnitude is the combination of the flux from the source, the lens and star 123NE. Fortunately, data of this field were also captured as part of the VVV survey although the event was still magnified. Data were obtained from the Vista telescope in JHK at the following epochs.

$$\begin{aligned} &H, \text{MJD} - \text{OBS} = 55423.1515 \\ &J, \text{MJD} - \text{OBS} = 55423.1576 \\ &K, \text{MJD} - \text{OBS} = 55423.1546. \end{aligned} \quad (1)$$

We use these data to determine whether the blend at the position of the source is consistent with the predicted source brightness. The image at the location of the source in the VVV image is a combination of the source, the lens, star 123NE and a star to the northwest. The brightness of these unrelated stars in the PSF is negligible when the source was amplified by 19.27 in *H* (where MJD − OBS = 55423.15153784 and MJD = JD − 2400000.5). We compare the flux ratios between the star at the position of the source and the 123 mas companion in the narrow Keck image and compare that with a calibrated wide Keck frame and that determined by CTIO/VVV.

In our Keck wide image, we cross-match to the stars in the VVV catalogue[31]. Both wide and narrow cameras on the NIRC2 result in an image with dimensions of 1,048 × 1,048 pixels. The wide image has a FOV of 40 arcsec, whereas the narrow image has a FOV of 10 arcsec. The narrow images were taken in sequence with a dither of 0.7 arcsec. The flux ratio between the source star and 123 mas companion is as follows.

$$\begin{aligned} &2018, K = 0.42 \\ &2015, H = 0.33 \\ &2016, H = 0.34. \end{aligned} \quad (2)$$

Using the flux ratio from the 2018 *K*-data and the predicted source *K*-brightness of $K_s = 17.17 \pm 0.04$, we determine the sum of the source and 123 mas companion to be $K = 16.79 \pm 0.04$, which is compatible with $K_{\rm Blend} = 16.78 \pm 0.03$ determined from only the 2015 Keck wide co-added frame. This indicates that there is no additional flux at the position of the source and that all of the photons from that object come from the source.

Light curve model

Since the publication of the MOA-2010-BLG-477Lb discovery paper[12], the MOA group has developed detrending methods[32,33] that can remove systematic errors due to the colour dependence of atmospheric refraction. We expect a significant colour-dependent differential refraction signal due to a bright main-sequence star at $I = 13.5$ that is only 3 arcsec from the MOA-2010-BLG-477 source star, and we have found a significant correction using a previously published method[33]. The resulting fitted light-curve is shown in Extended Data Fig. 4 while the best-fit model parameters using these new data are shown in Extended Data Table 1. Three of these parameters also apply to single-lens models. These are the Einstein radius crossing time (t_E), the time of closest approach (t_0) between the source and lens centre of mass, and the distance of this closest approach (u_0) in units of Einstein radius. A binary lens requires three additional parameters, namely, the lens separation (s) in units of the Einstein radius, the angle between lens separation and source trajectory (α) and the planet–star mass ratio (q). Events such as MOA-2010-BLG-477 with caustic crossings require the source radius crossing time (t^*) to account for finite source effects. Finally, it is also important to include parameters to describe the orbital motion of the lens system and the Earth-based observers. The orbital period of the planet is many years; therefore, the only detectable effect of orbital motion is the relative lens velocities $\dot{s}_x$ and $\dot{s}_y$ in directions parallel and perpendicular to the lens separation, respectively. The microlensing parallax is described by the north and east components of the microlensing parallax vector, π_E. The inclusion of microlensing parallax introduces an approximate degeneracy that corresponds to a flip in the orientation of the lens system with respect to the orientation of the Earth's orbit. We label the solutions with the sign of the u_0 parameter. The $u_0 > 0$ model is favoured by $\Delta\chi^2 = 5.08$, and it is displayed in Extended Data Fig. 6, but both models are compatible with our overall conclusions. A comparison of the cumulative $\Delta\chi^2$ for a model with and without parallax and orbital motion is shown in Extended Data Fig. 5.

One major difference between the analysis in the discovery paper[12] and our new analysis is that the Einstein ring crossing time, t_E, has decreased by about 16%. This causes a similar increase in the mass ratio q, because the timescale of the planetary signal has not changed. The other significant change in the model parameters can be found in the microlensing parallax values. As shown in Extended Data Fig. 6a, only one component of the microlensing parallax vector, π_E, is tightly constrained by the data. It is fairly common for the component parallel to the direction of the Earth's acceleration at the time of the event to be measured much more precisely than the perpendicular component; in this case, the uncertainty in the perpendicular component is increased by the degeneracy between the microlensing parallax and lens orbital motion. This parallel component is roughly in the the east–west direction for events in the Galactic bulge. However, the full π_E can be determined[34,35] with a measurement of the lens–source relative proper motion, $\mu_{\rm rel,G}$, although this must be be done in the geocentric frame that has been used for the light curve modelling.

Although changes in the model due to the improved MOA data are fairly noticeable, they have very little effect on our conclusions. We have performed the full analysis using the light curve models from the discovery paper[12], and these suggested very similar results. The only difference is that the old analysis shifted the $\pi_{E,E}$ towards more positive values by 0.1–0.2. As a result, the old light curve analysis allowed higher-mass host stars.

We note that the discovery paper suggested that it might be sensible to search for three-body lens systems that could explain this light curve. However, unlike the case of published triple-lens events[36–39], this light curve shows no evidence of an unmodelled light curve feature that can be explained by an additional lens. Thus, we can expect that the only effect of an additional lens would be to increase the uncertainties in the properties of the lens masses in the binary lens model[40], usually by very small amounts. As our primary conclusions are based on the properties of the host star, an additional lens that is consistent with the data would not affect our conclusions.

Bayesian analysis of light curve models with a Galactic prior

Our analysis makes use of the light curve models from the Markov chain Monte Carlo calculations from our re-analysis of the MOA data with our detrending method[33], as well as other datasets from the discovery paper[12]. These models incorporate the effects of the orbital motion of Earth that are responsible for the microlensing parallax, as well as the orbital motion of the planet. The microlensing parallax is a two-dimensional vector, π_E, parallel to the lens–source relative proper motion, which means that the distribution of microlensing parallax vectors from the light curve models constrains the direction of the lens–source relative proper motion. The amplitude of the lens–source relative proper motion vector is determined by finite source effects in the microlensing light curve. However, the direction and length of these lens–source relative proper motion vectors are not determined in the heliocentric reference frame that is appropriate for high-angular-resolution follow-up Keck observations. The light curve models use a geocentric reference frame that moves with the velocity of the Earth at the time of closest lens–source alignment. For MOA-2010-BLG-477, this velocity is $v_{N,E} = (-2.7933, 19.5634)$ km s^{-1}, and the transformation to the relative proper motion in the heliocentric reference frame, $\mu_{rel,H}$, is given in refs. [34,41], where the relative parallax is given by $\pi_{rel} = \mathrm{AU}/D_L - \mathrm{AU}/D_S$. This transformation from $\mu_{rel,G}$ to $\mu_{rel,H}$ cannot be computed only with the light curve parameters as π_{rel} depends on the source and lens distances. Therefore, we must invoke the Galactic model to properly sample the source distance (D_S) values. We have used the Galactic model from ref. [17] in our analysis. Our results are largely independent of the choice of the Galactic model for this Bayesian analysis. The only poorly understood prior is the host-mass dependence of the planet-hosting probability, because we are considering a lens that is known to host a planet. For simplicity, we assume that all of the white dwarfs are equally probable to host a planet. Once the source distance is selected, the lens distance can be determined from the following light curve parameters.

$$\mu_{rel,H} = \mu_{rel,G} + \frac{\boldsymbol{v}_{\oplus N,E}}{\mathrm{au}}\pi_{rel}, \quad (3)$$

$$D_L = \frac{AU}{\pi_E \theta_E + \mathrm{au}/D_S}. \quad (4)$$

Although π_E is only partially constrained by the light curve data, it is precisely determined for each model in the Markov chain; therefore, equation (4) can be used for each Markov chain model. The Galactic model also provides weights for the density of stars at the distance to the lens, D_L, and by the probability of a star with a mass equal to the lens mass. This implicitly includes the assumption that all stars are equally probable to host the planet of the measured mass ratio and projected separation.

Extended Data Fig. 6 shows how the Galactic model affects the distributions of the π_E and $\mu_{rel,H}$ vectors. Extended Data Fig. 6a, b shows the π_E distribution from the light curve models in ref. [12] and the implied $\mu_{rel,H}$ distribution, with the help of the D_S distribution from the Galactic model in ref. [17]. The component of π_E parallel to the direction of the Earth's acceleration during the event is tightly constrained. This component is close to the east direction. Conversely, the perpendicular component, which is largely in the north–south direction, is very weakly constrained. Extended Data Fig. 6 shows the result when we apply the complete Galactic model including the mass function for main-sequence stars. This removes the light curve models with small π_E values and therefore large masses. It was these low-π_E, high-mass light curve models that allowed the π_E vector to point in any direction. This was responsible for the ring distribution of $\mu_{rel,H}$, but with the high-mass lens systems excluded, this ring is broken into two arcs to the north and south, with low-mass lens systems only allowed in the northern arc. Our Keck observations have ruled out any main-sequence stellar lenses in these arcs. Our model does assume that stars with masses above $1.1M_\odot$ have left the main sequence, but such stars would also be brighter than the source star, which are clearly ruled out over the full ring shown in Extended Data Fig. 6b.

With main-sequence hosts ruled out, we can now turn our attention to white-dwarf host stars for the MOA-2010-BLG-477Lb exoplanet. We can repeat the same calculation that we did for main-sequence sources. This requires a mass–luminosity distribution for white dwarfs. We construct such a distribution from the 20 pc sample as in ref. [18], excluding unresolved binary white dwarfs because these probably have unreliable parameters. The resulting white dwarf mass–luminosity relation, constructed using a multivariate Gaussian kernel density estimation is shown in Extended Data Fig. 3. The results of a repeat of the Bayesian analysis with the main-sequence mass function replaced by our white-dwarf mass function, from Extended Data Fig. 3, is shown in Extended Data Fig. 6e, f. The results are similar to the main-sequence case, but the exclusion of low-π_E, high-mass light curve models is now slightly stronger because the white-dwarf mass function strongly peaks at around $M_L \approx 0.57–0.58M_\odot$. This Bayesian analysis is also used to produce the lens-system properties presented in Table 1. The contours from Extended Data Fig. 6f are reproduced in Extended Data Fig. 7c, where they replace the contours for the main sequence stars shown in Fig. 1c.

Detection limits and PSF deconvolution

We determine the detection threshold of our Keck images by estimating the flux of a point source and evaluating the normalized cross-product with the PSF. We obtain this quantity for all of the points in the subtracted image and construct a map of the amplitudes. To obtain an estimate of the fluctuations due to noise, we calculate the standard deviation in this map. We consider that these fluctuations are significant at the 3σ level and this level is our detection limit. We then convert this 3σ limit into magnitude and obtain a minimum limit of detection of $H \simeq 21.1$.

Although the relative proper motion indicates that the lens is distinct from the PSF of the source star, we then perform an analysis to determine whether the star at the position of the source is consistent with a single object or whether there is evidence of a two-component system. To do this, we generate a numerical estimate of the PSF by stacking the brightest stars in the neighborhood of our target. The accurate position of each PSF is estimated by iterative Gaussian-weighted centring. The PSFs are then interpolated, re-centered and stacked, and the median solution is obtained. In our *H*-band images, the star of interest is close to the star to the northeast, which means that it may receive some contribution from the PSF wings of its neighbour. To subtract any neighbour contributions, we reconstruct the wings of the PSF of the more distant star as a single function of distance and subtract this weak contribution from the image. Then, the best solution obtained is subtracted, leaving only the stars of interest. The result of this subtraction and the residuals are presented in Extended Data Fig. 2.

When reconstructing a single star, a common problem is to determine whether this star is a single PSF or a very close system of multiple PSFs. For example, if the single PSF fit results in significant residuals, it is clear that the fit of a binary system should be attempted. In this case, constraints on the PSF can be used to find upper limits on the allowed separations that are compatible with the data and noise. Our method to achieve this and to overcome the degeneracy created when the PSF components are very close are described below.

The image is shown in Extended Data Fig. 2; I_C is the result of the convolution of the object data and I_0, with the PSF (ϕ). Let us consider the case where the un-convolved data I_0 is very narrow with respect to the PSF, which is typical in cases of two close-together stars. In this instance, we can write the following.

$$I_C(x,y) = \int \phi(x-u, y-v) I_0(u,v) \mathrm{d}u\mathrm{d}v \quad (5)$$

Considering that the variations are small with respect to the variations of ϕ, we can write ϕ as a local expansion in the local variables (u,v).

$$I_C(x,y) \simeq m_0\phi(x,y) - m_1\frac{\partial\phi}{\partial x} - m_2\frac{\partial\phi}{\partial y} + m_3\frac{\partial^2\phi}{\partial x^2} + m_4\frac{\partial^2\phi}{\partial x\partial y} + m_5\frac{\partial^2\phi}{\partial y^2} \quad (6)$$

Here

$$\begin{aligned} m_0 &= \int I_0(u,v)\mathrm{d}u\mathrm{d}v \\ m_1 &= \int I_0(u,v)u \ \ \mathrm{d}u\mathrm{d}v \\ m_2 &= \int I_0(u,v)v \ \mathrm{d}u\mathrm{d}v \\ m_3 &= \frac{1}{2}\int I_0(u,v)u^2\mathrm{d}u\mathrm{d}v \\ m_4 &= \int I_0(u,v)uv \ \ \mathrm{d}u\mathrm{d}v \\ m_5 &= \frac{1}{2}\int I_0(u,v)v^2\mathrm{d}u\mathrm{d}v \end{aligned} \quad (7)$$

The m_1 and m_2 coefficients represent the degrees of freedom related to the centre of the function I_0. To eliminate these degrees of freedom, we make the centre of flux of I_0 coincide with the origin of the coordinate system. In this case, $m_1 = 0$ and $m_2 = 0$. As such, we are left with an expansion with four basis functions, the PSF and its three second-order derivatives. The moments of the function I_0 are simply the three coefficients (m_3, m_4, m_5) normalized by the total flux (note that if the PSF is normalized, the total flux and coefficient m_0 should be very similar).

We use the numerical model of the PSF to reconstruct the derivatives up to the second order. The derivatives are obtained by shifting the PSF model and taking the difference with the original PSF. The value of the shift is small with respect to the size of the PSF grid. We choose a value of 0.010, but we also tested 0.100 and 0.001, and no significant changes were observed. In creating the PSF model, we take an area around the object large enough to include the PSF wings but small enough to avoid including another object.

Data availability

The Keck Observatory data used in this study are freely available in the Keck Observatory Archive (https://koa.ipac.caltech.edu/cgi-bin/KOA/nph-KOAlogin). Data from the VISTA Variables in the Via Lactea (VVV) survey are available in the European Southern Observatory archive (http://archive.eso.org/wdb/wdb/adp/phase3_main/form?phase3_collection=VVV&release_tag=6). Data used to model the light curve are available from the corresponding author upon reasonable request.

Code availability

The Keck pipeline is available on GitHub (https://github.com/blackmanjw/KeckPipeline). The Bayesian analysis code of D.P.B. uses routines from ref. [42], which are subject to restricted availability.

24. Vandorou, A. et al. Revisiting MOA 2013-BLG-220L: a solar-type star with a cold super-Jupiter companion. *Astron. J.* **160**, 121 (2020).
25. OGLE Extinction Calculator. http://ogle.astrouw.edu.pl/cgi-ogle/getext.py (2013).
26. Nataf, D. M. et al. Reddening and extinction toward the galactic bulge from OGLE-III: the Inner Milky Way's R_V ~ 2.5 extinction curve. *Astrophys. J.* **769**, 88 (2013).
27. Blackman, J. W. et al. Confirmation of the stellar binary microlensing event, Macho 97-BLG-28. *Astrophys. J.* **890**, 87 (2020).
28. Beaulieu, J.-P. et al. Revisiting the microlensing event Ogle 2012-Blg-0026: a solar mass star with two cold giant planets. *Astrophys. J.* **824**, 83 (2016).
29. Bertin, E. SWarp: resampling and co-adding FITS images together. *Astrophysics Source Code Library record no. ascl:1010.068* (2010).
30. Bertin, E. & Arnouts, S. SExtractor: software for source extraction. *Astron. Astrophys. Sup.* **117**, 393–404 (1996).
31. Minniti, D. et al. VISTA Variables in the Via Lactea (VVV): the public ESO near-IR variability survey of the Milky Way. *New Astron.* **15**, 433–443 (2010).
32. Bennett, D. P. et al. Planetary and other short binary microlensing events from the MOA short-event analysis. *Astrophys. J.* **757**, 119 (2012).
33. Bond, I. A. et al. The lowest mass ratio planetary microlens: OGLE 2016–BLG–1195Lb. *Mon. Not. R. Astron. Soc.* **469**, 2434–2440 (2017).
34. Bhattacharya, A. et al. WFIRST exoplanet mass-measurement method finds a planetary mass of 39 ± 8 M for OGLE-2012-BLG-0950Lb. *Astronom. J.* **156**, 289 (2018).
35. Bennett, D. P. et al. Keck observations confirm a super-Jupiter planet orbiting M dwarf OGLE-2005-BLG-071L. *Astronom. J.* **159**, 68 (2020).
36. Gaudi, B. S. et al. Discovery of a Jupiter/Saturn analog with gravitational microlensing. *Science* **319**, 927–930 (2008).
37. Bennett, D. P. et al. Masses and orbital constraints for the OGLE-2006-BLG-109Lb,c Jupiter/Saturn analog planetary system. *Astrophys. J.* **713**, 837–855 (2010).
38. Gould, A. et al. A terrestrial planet in a ~1-au orbit around one member of a ~15-AU binary. *Science* **345**, 46–49 (2014).
39. Bennett, D. P. et al. The first circumbinary planet found by microlensing: OGLE-2007-BLG-349L(AB)c. *Astronom. J.* **152**, 125 (2016).
40. Zhu, W. et al. Empirical study of simulated two-planet microlensing events. *Astrophys. J.* **794**, 53 (2014).
41. Dong, S. et al. First space-based microlens parallax measurement: Spitzer observations of OGLE-2005-SMC-001. *Astrophys. J.* **664**, 862–878 (2007).
42. Press, W., Teukolsky, S., Vetterling, W. & Flannery, B. *Numerical Recipes* (Cambridge Univ. Press, 1992).

Acknowledgements Data presented in this work were obtained at the W. M. Keck Observatory from telescope time allocated to the National Aeronautics and Space Administration through the agency's scientific partnership with the California Institute of Technology and the University of California. This work was supported by the University of Tasmania through the UTAS Foundation, ARC grant DP200101909, and the endowed Warren Chair in Astronomy. We acknowledge the support of ANR COLD WORLDS (ANR-18-CE31-0002) at the Institut d'Astrophysique de Paris and the Laboratoire d'Astrophysique de Bordeaux. D.P.B., A.B., N.K., C.R. and S.K.T. were supported by NASA through grant NASA-80NSSC18K0274 and by NASA award no. 80GSFC17M0002. E.B. acknowledges support from NASA grant 80NSSC19K0291. Work by N.K. is supported by JSPS KAKENHI grant no. JP18J00897. C.D. acknowledges financial support from the State Agency for Research of the Spanish MCIU through the 'Center of Excellence Severo Ochoa' award to the Instituto de Astrofísica de Andalucía (SEV-2017-0709), and the Group project ref. PID2019-110689RB-I00/AEI/10.13039/501100011033. D.V. gratefully acknowledges the support of the STFC via an Ernest Rutherford Fellowship (grant ST/P003850/1).

Author contributions J.W.B. led the photometric and formal analysis and wrote the manuscript. J.W.B., V.B. and J.P.B. took and reduced the photometric data using a pipeline written by J.W.B. and A.V. with contributions from J.B.M. for magnitude calibrations. D.P.B., J.P.B. and A.A.C. discussed the conceptual and analysis approaches. D.P.B. was the principle investigator of the Keck telescope proposal, led the planning of the observations, and conducted the light curve modelling and Bayesian analyses. C.D. provided insight into single and double white-dwarf planetary systems. I.B. processed the detrended MOA photometry. A.B. and E.B. assisted with proper motion calculations. A.B. and N.K. assisted with observing on Keck. C.R. calculated the parallax, proper motion and lens prediction contours. C.A. worked on the PSF analysis and the determining of detection limits. D.P.B., J.P.B., A.A.C., C.D., S.K.T. and D.V. contributed to the review and editing of the manuscript.

Competing interests The authors declare no competing interests.

Additional information
Supplementary information The online version contains supplementary material available at https://doi.org/10.1038/s41586-021-03869-6.

Correspondence and requests for materials should be addressed to J. W. Blackman.

Peer review information *Nature* thanks Albert Zijlstra and the other, anonymous, reviewer(s) for their contribution to the peer review of this work. Peer reviewer reports are available.

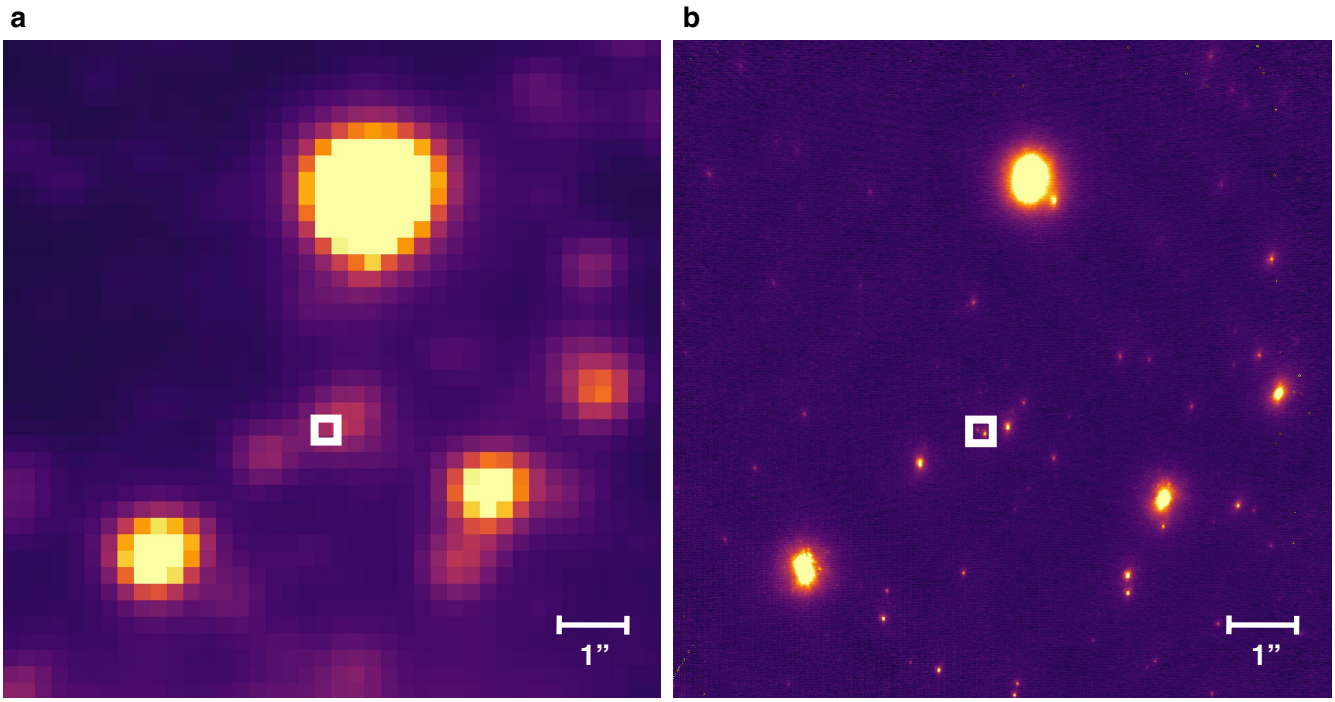

Extended Data Fig. 1 | OGLE-III and Keck imaging of MOA-2010-BLG-477Lb. (**a**) OGLE-III image of the OGLE-BLG176.8 field (**b**) H-band image of the same field taken in 2015 with Keck/NIRC2 with the narrow camera.

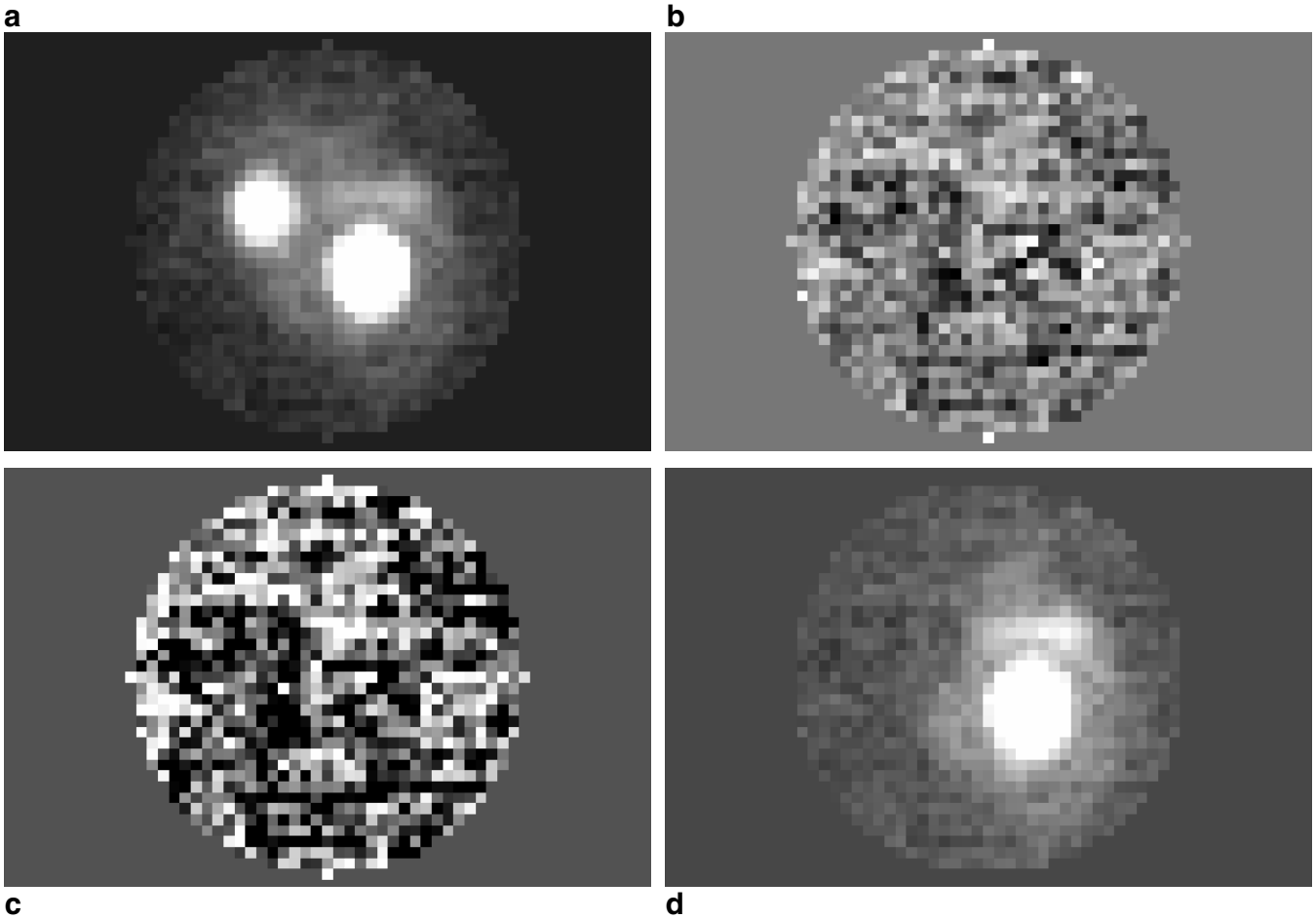

Extended Data Fig. 2 | Keck Point Spread Function (PSF) fit and residuals. (**a**) Keck/NIRC2 H-band image from 2018. (**b**) Residuals after fitting the PSF using multiple stars in the neighbourhood of the source. Both the object to the north-east (upper left in panel A) and the object at source position (lower right) are subtracted using this PSF fit. There is no structure or indication of a double star in either of the two objects. (**c**) The residuals from panel B normalized to the Poisson noise. (**d**) Panel A but subtracting the fitted PSF from the unrelated companion.

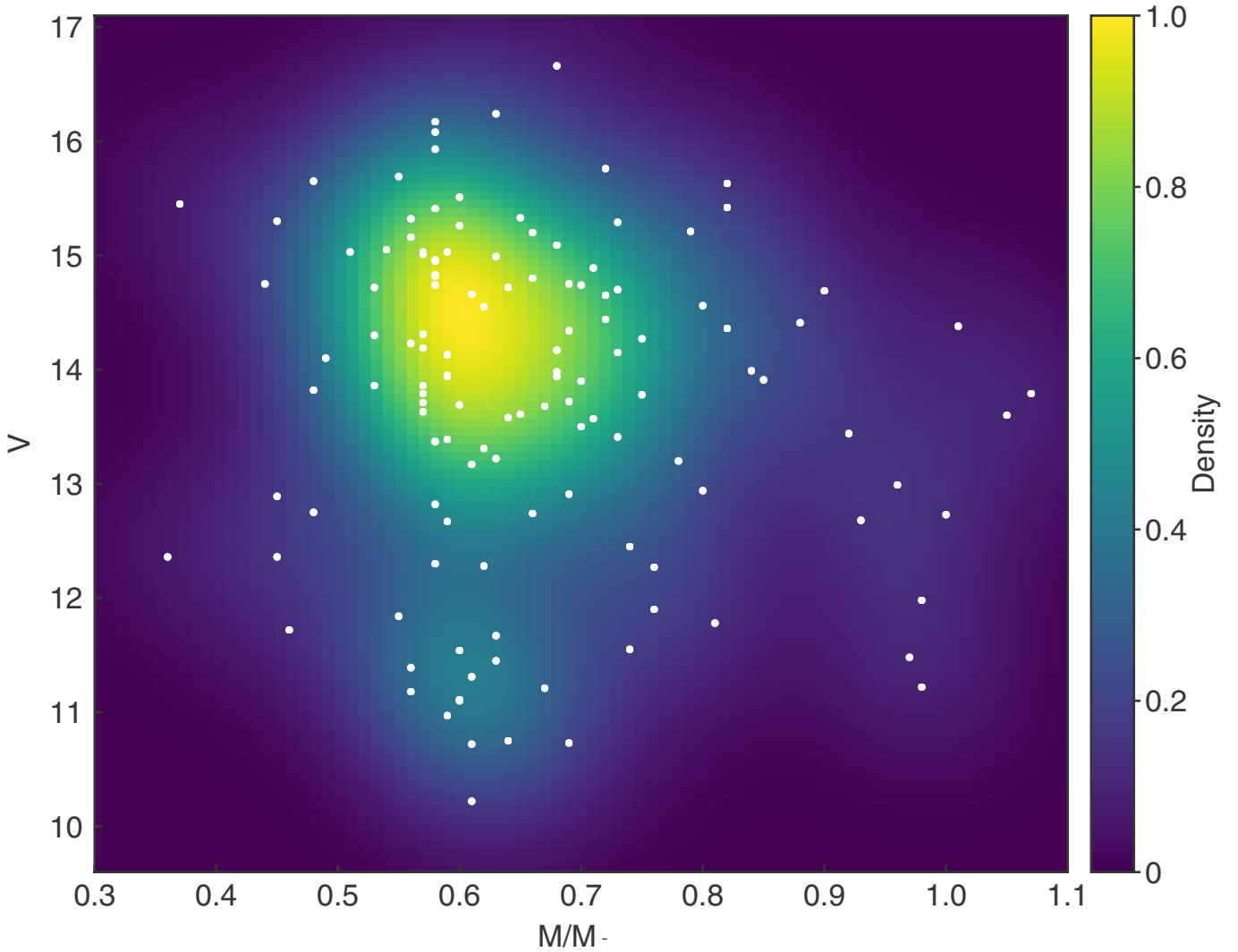

Extended Data Fig. 3 | White Dwarf Mass-Luminosity distribution derived a sample of 130 white dwarfs from a homogeneous and complete sample of white dwarfs within 20pc of the Sun[18]. Two unresolved double-white dwarfs (DWD), eight unresolved DWD candidates and one unresolved binary white dwarf with a main-sequence companion have been removed from this sample[19]. 14 stars with distances > 20 pc have also been removed. The white dots indicate the masses and *V* band magnitudes of the white dwarfs in this sample, and the color distribution indicates the smooth Gaussian multivariate kernel-density distribution that we have used in our analysis.

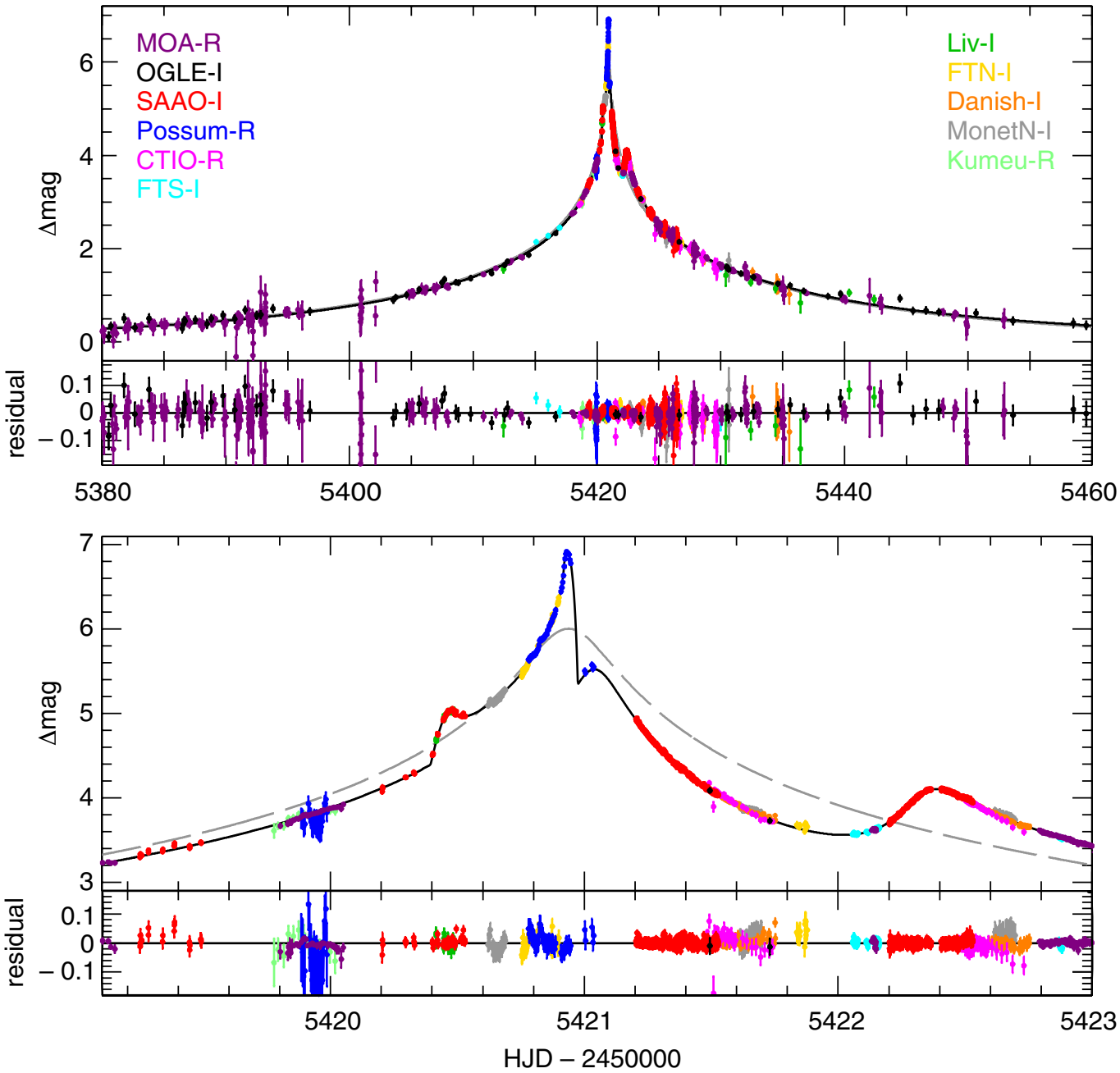

Extended Data Fig. 4 | Light Curve Data and Model for microlensing event MOA-2010-BLG-477. The solid curve is the best fit model and the dashed grey curve is the single lens model with the same single lens parameters. The different colors represent different data sets from different telescopes. One sigma error bars are shown. The data sets are explained in the discovery paper[12].

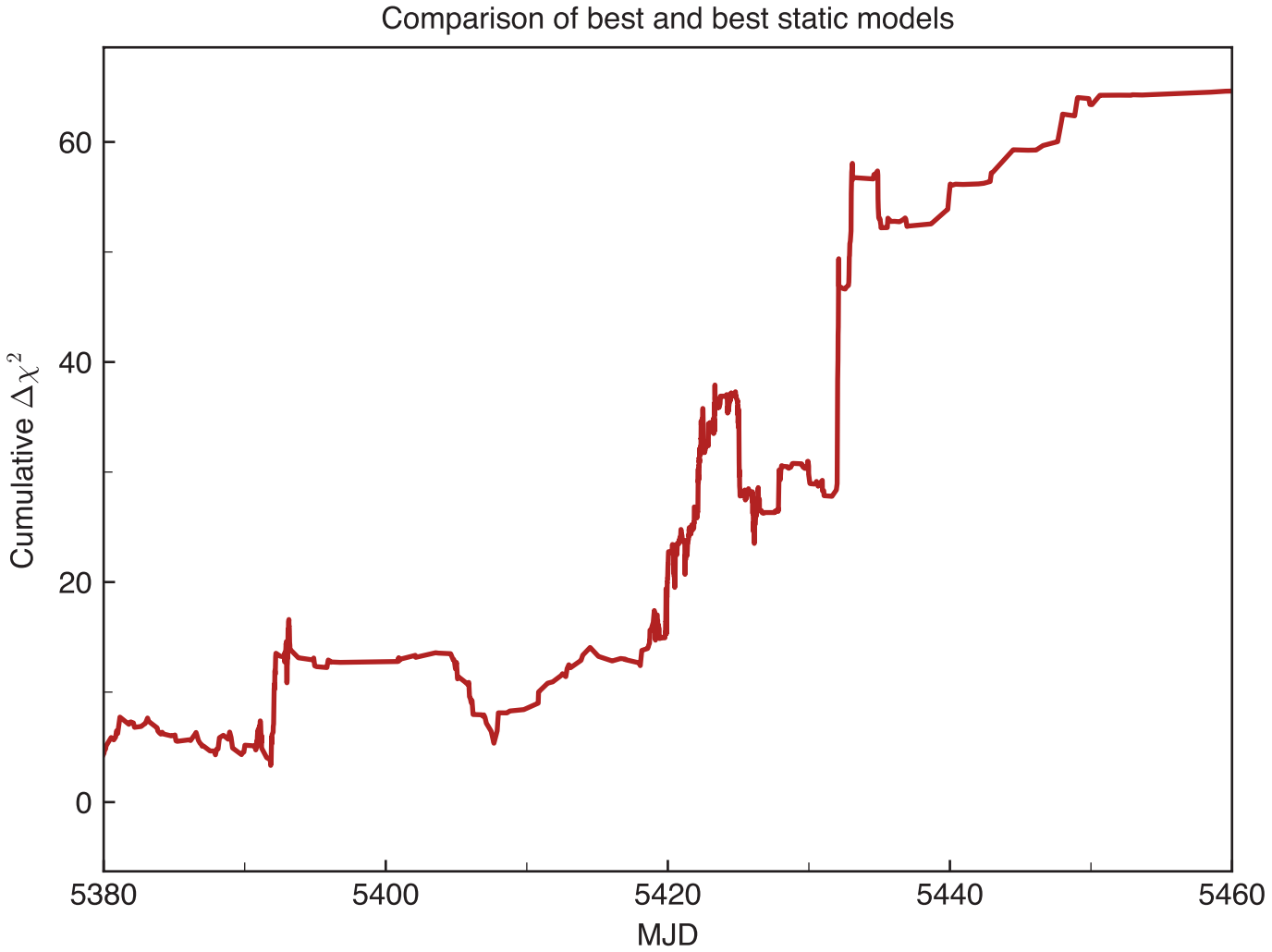

Extended Data Fig. 5 | Cumulative $\Delta\chi^2$ comparing a static light curve model with that including parallax and orbital motion. The bulk of the signal comes following the light curve peak. The parallax plus orbital motion comes primarily from the MOA data ($\Delta\chi^2 = 45$) and the SAAO data ($\Delta\chi^2 = 9.0$).

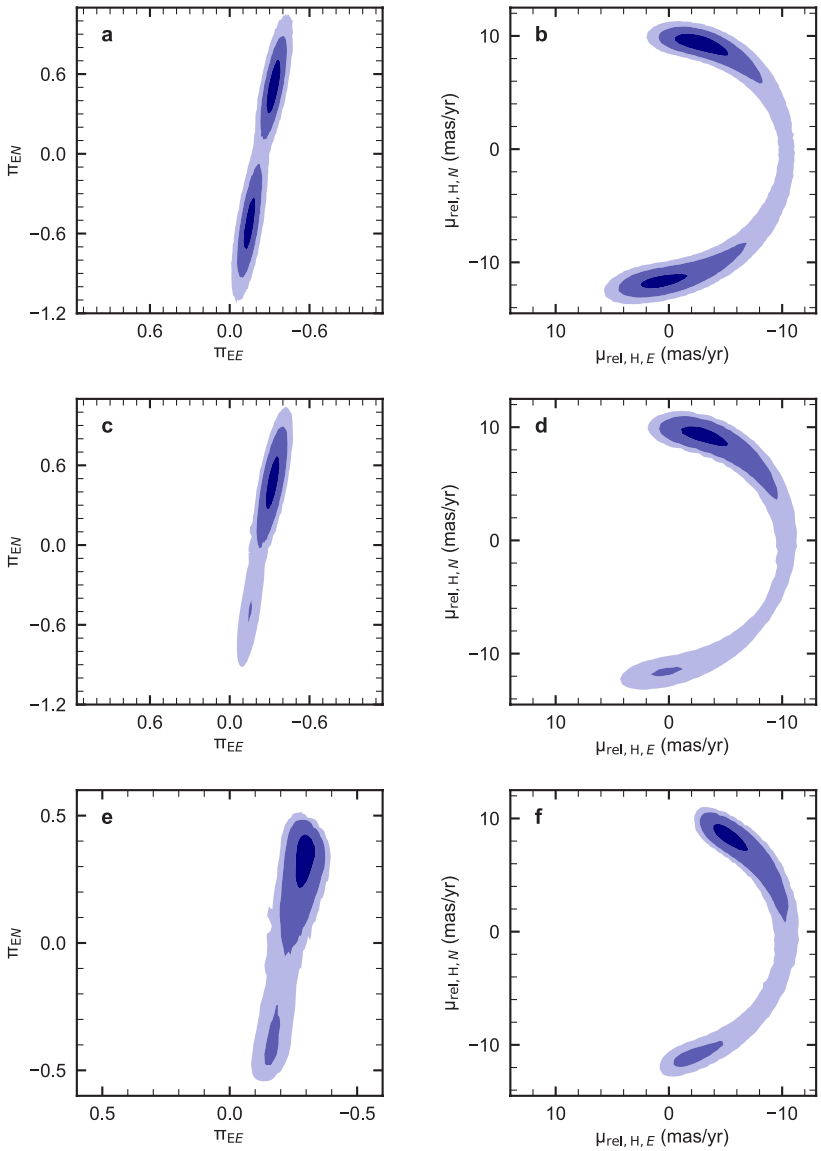

Extended Data Fig. 6 | Predictions of the microlens parallax vector π_E and the corresponding predicted relative lens-source proper motion μ_{rel} for a main sequence and white dwarf lens. Based on a Markov-Chain Monte-Carlo (MCMC) analysis using Galactic model priors as in[17], the upper panels (**a**) and (**b**) show the unweighted predicted components of (π_{EN}, π_{EE}) and ($\mu_{rel,HN}$, $\mu_{rel,HE}$). The middle panels (**c**) and (**d**) show the weighted predictions for a main-sequence lens. The lower panels (**e**) and (**f**) show the weighted predictions for a white-dwarf lens. The three shades of blue from dark to light denote probabilities of of 0.393, 0.865, 0.989. When integrating over all parameters the limit of the 0.393 contour corresponds to the 1σ distribution of any chosen parameter.

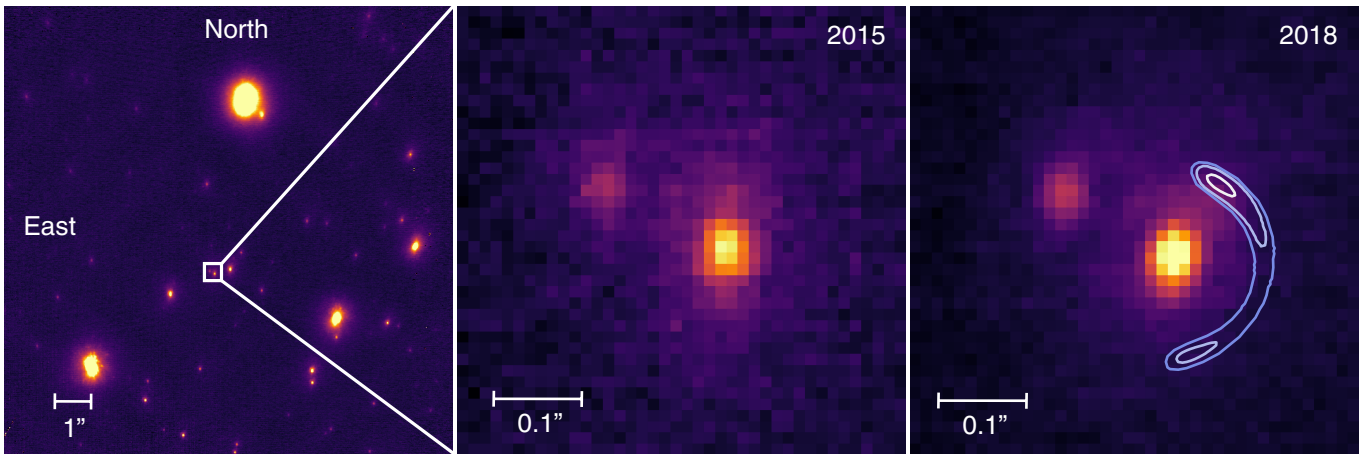

Extended Data Fig. 7 | H-band adaptive optics imaging from the KECK observatory, with contours showing the predicted position of a white dwarf lens (analogous to Fig. 1) (**a**) A crop of a narrow-camera H-band image obtained with the NIRC2 imager in 2015 centered on MOA 2010-BLG-477 with an 8 arcsec field of view. (**b**) A 0.36 arcsec zoom of the same image. The bright object in the center is the source. To the north-east (the upper left) is an unrelated $H = 18.52 \pm 0.05$ star 123 mas from the source. (**c**) The field in 2018. The contours indicate the likely positions of the white dwarf host (probability of 0.393, 0.865, 0.989 from light to dark blue) using constraints from microlensing parallax and lens-source relative proper motion.

Extended Data Table 1 | Best Fit Model Parameters

	This Analysis		Discovery Paper	
parameter	$u_0 > 0$	$u_0 < 0$	$u_0 > 0$	$u_0 < 0$
t_E (days)	39.523(425)	39.796(441)	46.868	47.560
t_0 (HJD′)	5420.9381(3)	5420.9376(3)	5420.9382	5420.9374
u_0	0.003966(51)	−0.003937(54)	0.003430	−0.003315
s	1.12203(52)	1.12278(51)	1.12407	1.12429
α (rad)	0.54126(176)	−0.54137(174)	0.54004	−0.53836
$q \times 10^3$	2.590(31)	2.587(31)	2.210	2.168
t_* (days)	0.02736(18)	0.02739(18)	0.02719	0.02719
$\dot{s}_x$	$0.00039^{+0.00021}_{-0.00030}$	$0.00030^{+0.00023}_{-0.00027}$	0.00223	0.00016
$\dot{s}_y$	$-0.00192^{+0.00099}_{-0.00146}$	$0.00274^{+0.00042}_{-0.00194}$	−0.00587	0.00196
$\pi_{\mathrm{E,N}}$	$0.4450^{+0.0750}_{-0.1499}$	$-0.5393^{+0.4053}_{-0.1524}$	0.5432	0.0974
$\pi_{\mathrm{E,E}}$	$-0.3165^{+0.0723}_{-0.0250}$	$-0.1467^{+0.0420}_{-0.0766}$	−0.1026	−0.0134
χ^2/dof	6420.91/6490	6425.97/6490	-	-

All errors are given as ± 1σ.